

1 **Validating Response of AC Microgrid to Line-to-Line Short Circuit in Islanded Mode** 2 **using Dynamic Analysis**

3

4

5

6 **Abstract**

7 This paper is presented in an attempt to validate the dynamic response of a microgrid to line-to-
8 line short circuit. The microgrid components include two identical Wind Turbine Generators
9 (WTGs) tied to a 100MVA, 13.8kV utility via a Point of Common Coupling (PCC). The utility-
10 microgrid testbed is modeled in SIMPOWERSystems® using two Doubly-Fed Induction
11 Generators (DFIGs) in the microgrid side. While in islanded operating mode, line-to-line short
12 circuit fault is applied at 6.0s and withdrawn at 8.0s, obtaining a 50.0s dynamic response of the
13 system for different fault locations, under voltage and reactive power control regimes of the wind
14 turbine controller. For measurement purpose, the absolute value of the stator complex voltage is
15 transformed to α, β, γ reference frame. Bidirectional power flow between the two feeders is
16 established in the study. The study also confirms that the microgrid composed of DFIGs offer
17 reactive power management capability, particularly by presenting superior performance when
18 stressed under Q control regime than under V control regime. Finally, the response of the testbed
19 to line-to-line short circuit has been validated and shown to be consistent with established short
20 circuit theory.

21

22 **Keywords:** Microgrid, Dynamic, DFIG, Microsource, Fault

23 **Abbreviations:** MS1 = Microsource 1, MS2 = Microsource 2, Feeder-a = Feeder connected to
24 microsource 1.

25

26 **1. Introduction**

27 The design and operation of power utility seek to generate, transmit and distribute electric power
28 in sufficiently large quantity and on uninterrupted basis to meet the contemporary and projected
29 future demands of the consumers in a load center. In order to achieve this goal, the system must
30 remain in operation continuously without long downtimes. Practically, achieving this goal
31 requires use of protective devices [1-4]. Protective devices function to achieve the following:

- 32 1. Minimize damage and repair costs whenever fault is sensed.
- 33 2. Safeguard the system to supply power continuously.
- 34 3. Consumer and personnel safety [5-9].

35 In order to meet above requirements, short circuit analyses are normally performed on the
36 system. The analysis will typically aim to determine the short-circuit rating of the equipment to
37 be purchased, installed and commissioned. Also, equipment manufacturers use the ratings

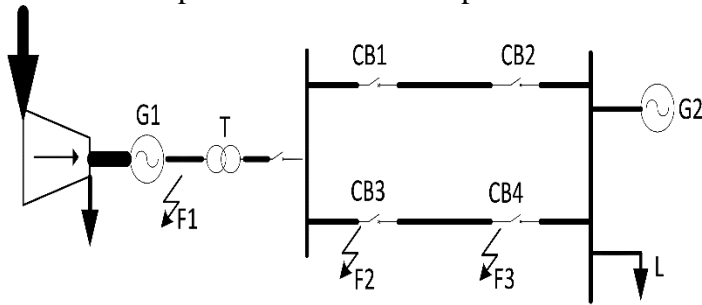
P(W) = Nominal active power in Watts; Q(VAr) = Nominal reactive power in Volt-Amp reactive

38 specified by their customers to ensure that their equipment are designed to satisfy client's safety
 39 and operational specifications under certain conditions for specified duration [10-13]. As the
 40 parameters of a power system and fault envelopes vary with time [14-16], short circuit analysis
 41 which depicts the system dynamics is useful in order to achieve the utility operational goals -
 42 ensuring high quality, continuous and safe delivery of power to consumers [17-20].

43 In this work, the authors present a utility-microgrid testbed for a research which aims at
 44 proposing a new microgrid protection. Since the protection to be developed would be based on
 45 measurement of three phase power, the nominal three phase active and reactive power is used and
 46 presented in this paper. Thus, this paper presents an attempt to validate the response of the
 47 modeled testbed to line-to-line short circuit. This is because the validity of the anticipated
 48 protection depends on the validity of the testbed's response to short circuit.

49 2. Short circuit in a power system

50 Consider a 3-phase to earth fault at point F2 as shown in fig. 1.



51
 52 **Fig. 1.** Typical power system with short circuit points F1, F2 and F3

53 In an electric power generator, fault current is often initially around 8 times the full-load current. It
 54 attenuates rapidly to around 5 times full-load current before attenuating less rapidly to less than full-load
 55 current value. In the direct axis, this results in three stages of fault current envelop named sub-transient
 56 (X_d''), transient (X_d') and steady-state (X_d) respectively.

57 Fault F2 is therefore seen as a modified generator fault which incorporates the effect of
 58 transformer T. The transformer reactance, X_T , is added to the reactances X_d'' , X_d' and X_d as
 59 given in (1), (2) and (3) [4, 6, 7, 20].

$$60 \quad x_d'' = X_d'' + X_T \quad (1)$$

$$61 \quad x_d' = X_d' + X_T \quad (2)$$

$$62 \quad x_d = X_d + X_T \quad (3)$$

63 The amplitude of the ac fault current in the sub-transient state, i_m'' , transient state, i_m' , and steady
 64 state, i_m^∞ , is presented in (4), (5) and (6), respectively.

$$65 \quad i_m'' = \frac{E_{fm}}{x_d''} \quad (4)$$

$$66 \quad i_m' = \frac{E_{fm}}{x_d'} \quad (5)$$

$$67 \quad i_m^\infty = \frac{E_{jm}}{x_d} \quad (6)$$

68 Addition of x_T attenuates the magnitude of the currents given in (4), (5) and (6). Secondly, the
 69 rate of dissipation of the stored magnetic energy is increased by the transformer resistance, R_T ,
 70 so that the dc component of short circuit current decays more rapidly. Thirdly, the time constants
 71 are increased by the transformer reactance as given in (7) and (8) [21-23].

$$72 \quad T_{d(network)}'' = T_d'' \left(\frac{X_d'}{X_d''} \right) \left(\frac{X_d'' + X_T}{X_d' + X_T} \right) \quad (7)$$

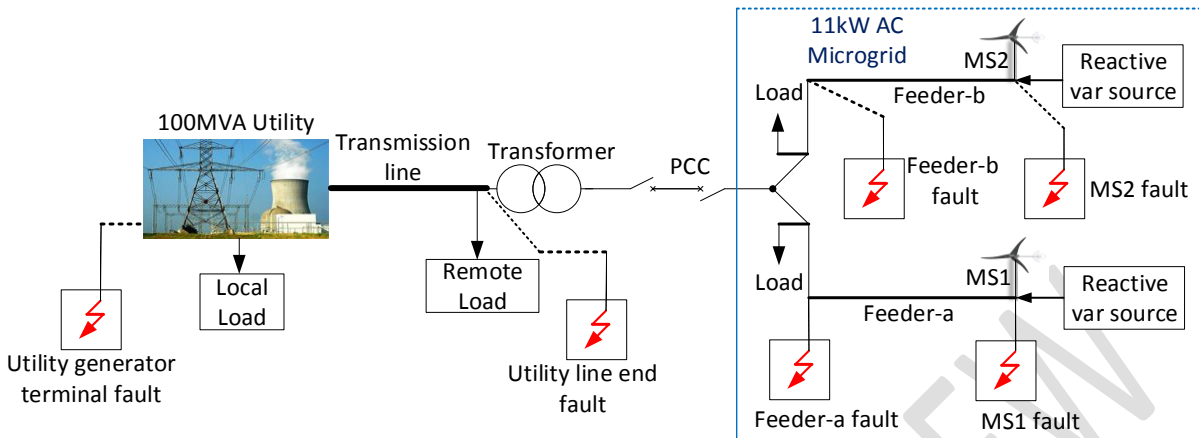
$$73 \quad T_{d(network)}' = T_d' \left(\frac{X_d'}{X_d'} \right) \left(\frac{X_d' + X_T}{X_d' + X_T} \right) \quad (8)$$

74 **3. Design of control systems**

75 The modeled system is subjected to small signal response analysis. It is found to be stable but its
 76 response time is unsatisfactory. Requisite regulators are then designed using closed-loop
 77 feedback structure. The systems designed are pitch angle regulator, active power management
 78 systems and reactive power management systems. The regulators are combined to implement
 79 two mutually exclusive control regimes. These two regimes are active power-voltage (V) control
 80 and reactive-active power (Q) control. Under power-voltage control, the controller maintains
 81 constant grid voltage with a 4% droop. Under reactive-active power control, the controller
 82 ensures constant reactive power at the grid.

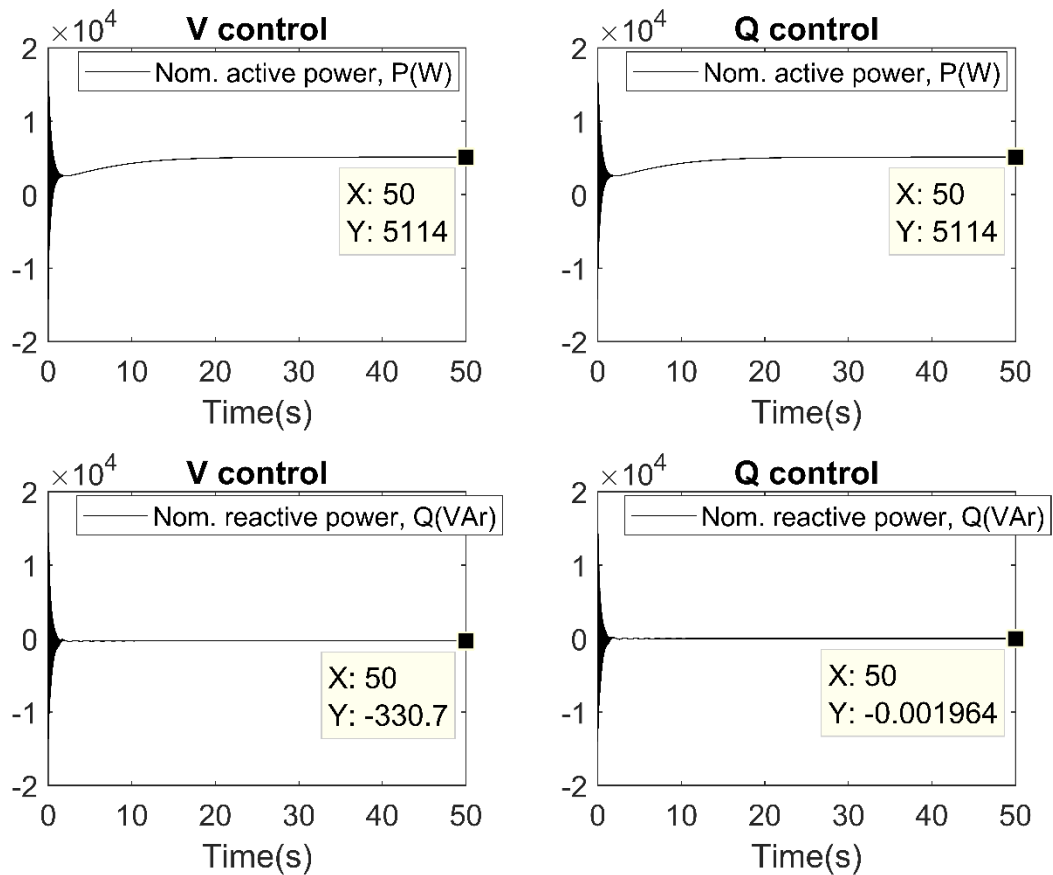
83 **4. Short circuit simulation and system dynamic response**

84 The testbed developed for this study is shown in fig. 2. In the network, each DFIG is nominally
 85 rated 5.5kW, 575V and linked to 2.5km highly resistive feeder (a or b). Each feeder is connected
 86 to the utility radially at the PCC. A modeled 20MVA STATCOM is connected to the utility side
 87 at the PCC. A local inductive load of 3.6MVA and a remote inductive load of 89.44MVA are
 88 serviced by the utility. A total inductive local load of 6.21kVA is serviced by the microgrid. The
 89 operating frequency of the system is 50Hz, with cut-in and cut-out wind speeds of 3ms^{-1} and
 90 6ms^{-1} , respectively. Islanding of the microgrid is achieved by opening the PCC.



91
92 **Fig. 2.** A basic diagram displaying the system under study

93 Fig. 3 shows the response of MS1 during normal operation under V and Q controls.
94



95
96 **Fig. 3.** Response of MS1 under normal operation in V and Q Controls

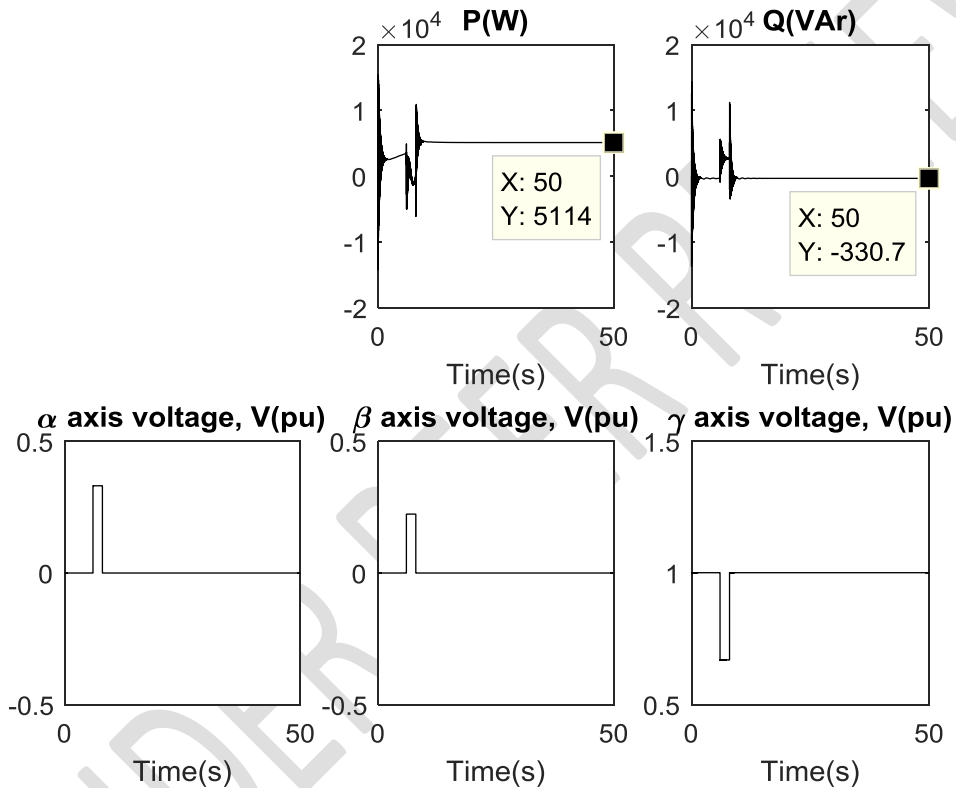
P(W) = Nominal active power in Watts; Q(VAr) = Nominal reactive power in Volt-Amp reactive

97 **5. Line-to-line short circuit**

98 Line-to-line short circuit fault is applied at 6.0s and withdrawn at 8.0s. Under this short circuit,
99 system's (microgrid feeders and DFIG) dynamics is simulated for 50.00s. The testbed's
100 responses for different fault locations and DFIG controller in voltage, V, and reactive power, Q,
101 control are obtained and presented in fig. 4 to fig. 19.

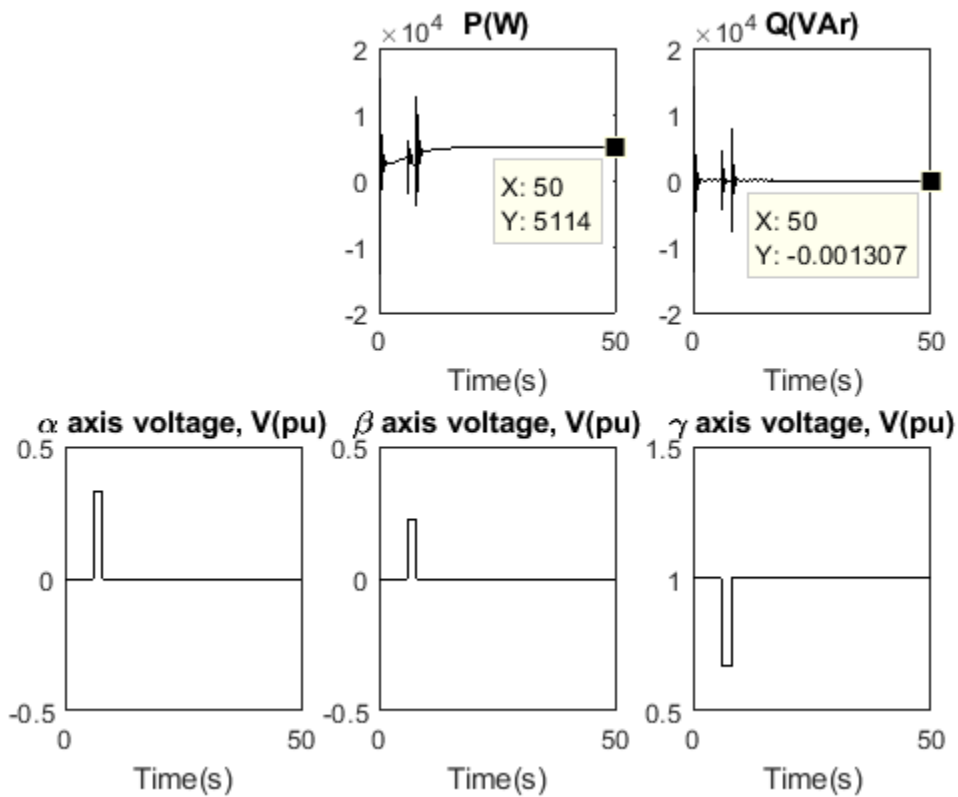
102 The responses of MS1 to short circuits at the terminals of utility generator under V and Q
103 controls are presented in fig. 4 and fig. 5, respectively.

104
105
106



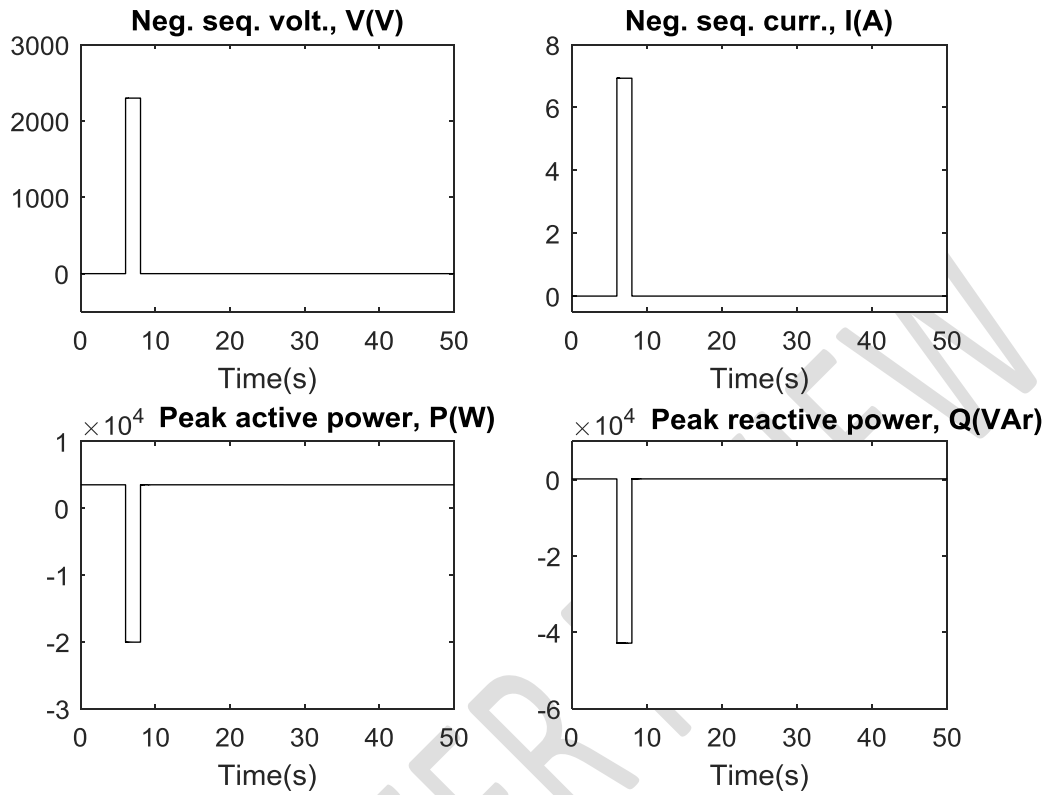
107
108 **Fig. 4.** Response of MS1 to L-L short circuit – V control
109

$P(W)$ = Nominal active power in Watts; $Q(VAr)$ = Nominal reactive power in Volt-Amp reactive



110
111 **Fig. 5.** Response of MS1 to L-L short circuit – Q control

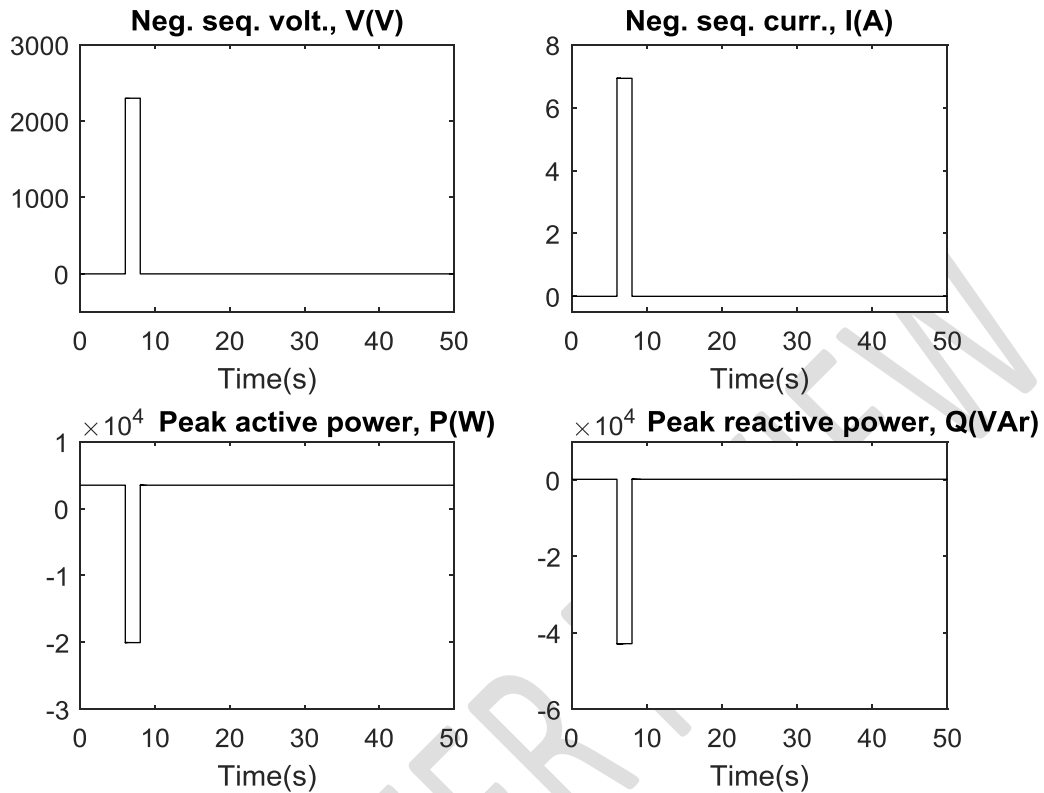
112
113 Fig. 6 shows response of feeder-a to short circuit at terminals of MS1 under V control, while fig.
114 7 shows response of same feeder to same short circuit under Q control.
115



116
117
118

Fig. 6. Response of feeder-a to L-L short circuit at terminals of MS1– V control

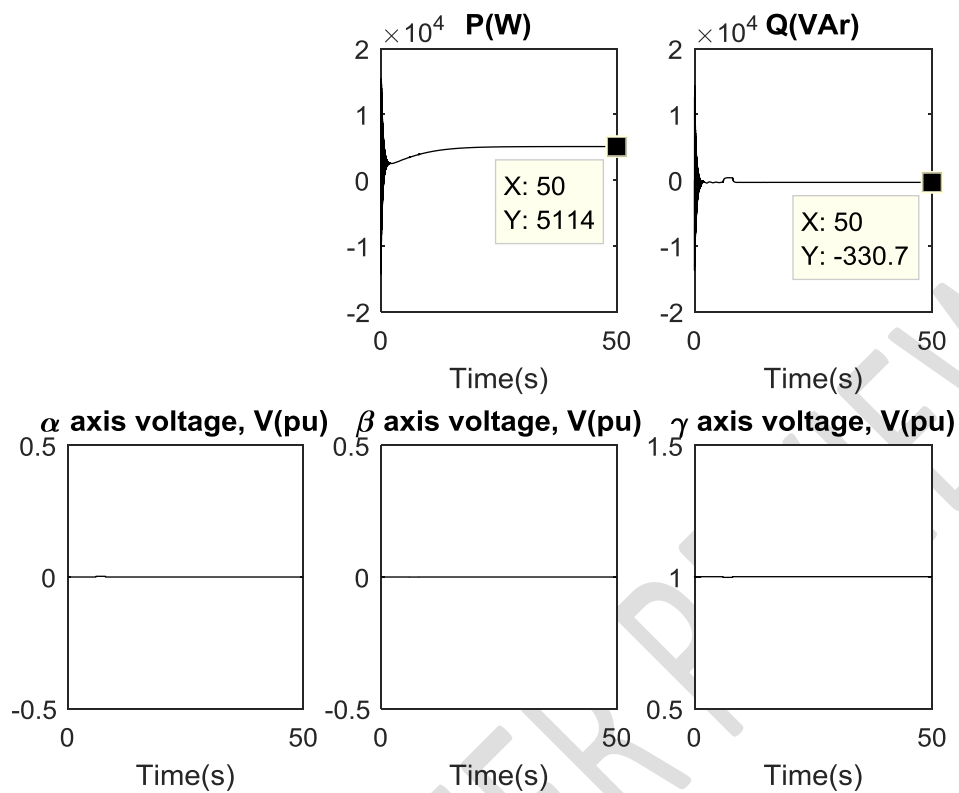
P(W) = Nominal active power in Watts; Q(VAr) = Nominal reactive power in Volt-Amp reactive



119 **Fig. 7.** Response of feeder-a to L-L short circuit at terminals of MS1– Q control
 120
 121

122 Note that under V control (fig. 4) when L-L short circuit is applied at its terminals, MS1 absorbs
 123 330.7 VAr from its reactive VAr compensator and that of MS2 at 50.00s. This is considerably
 124 higher than 0.001307 VAr it absorbs under Q control (fig. 5), indicative of reactive power
 125 management of DFIG as published by Moayed Moghbel et al. in [24] and in [25-27]. The peak
 126 active power of feeder-a rose to 20kW in a direction opposite the nominal active power flow
 127 direction during the fault, indicating active power support from MS2 and feeder-b to feed the
 128 fault point in feeder-a. Similarly, reactive power flow on feeder-a rose to more than 40k VAr in
 129 an opposite direction during the fault, as seen in fig. 6. Negative sequence quantities only exist
 130 during the fault, as depicted in fig. 6 and fig. 7.

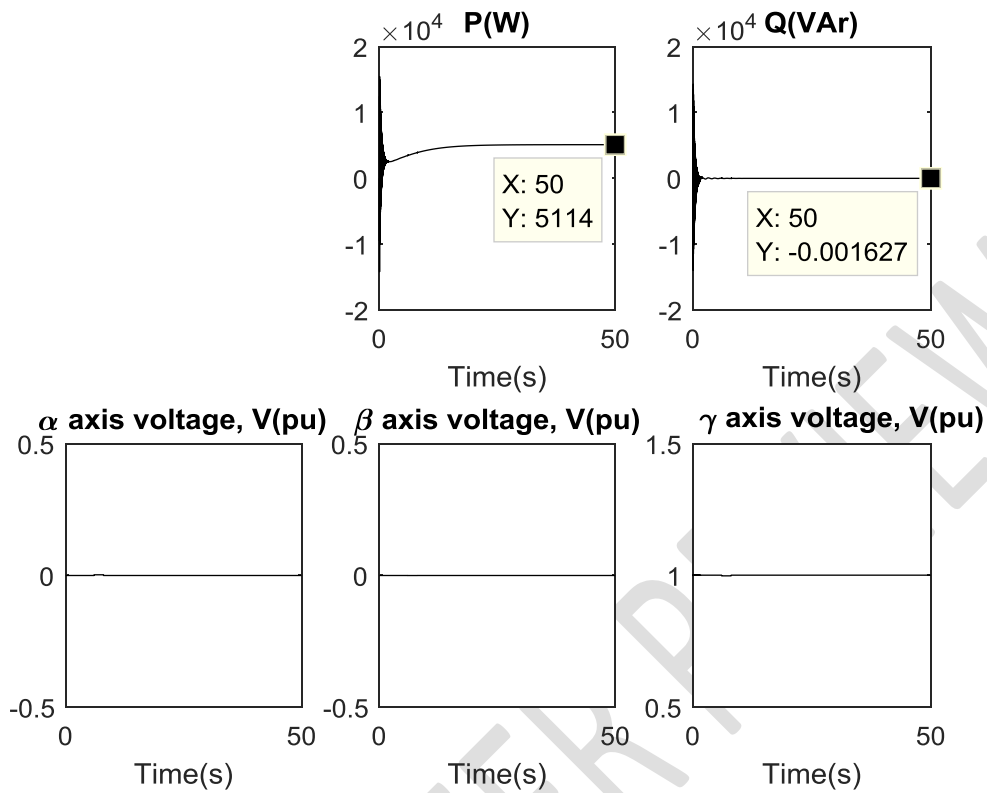
131 The responses of MS1 to short circuits at the ends of feeder-a under V and Q controls are
 132 presented in fig. 8 and fig. 9, respectively.
 133



134
135
136
137

Fig. 8. Response of MS1 to L-L short circuit at ends of feeder-a – V control

$P(W)$ = Nominal active power in Watts; $Q(VAr)$ = Nominal reactive power in Volt-Amp reactive

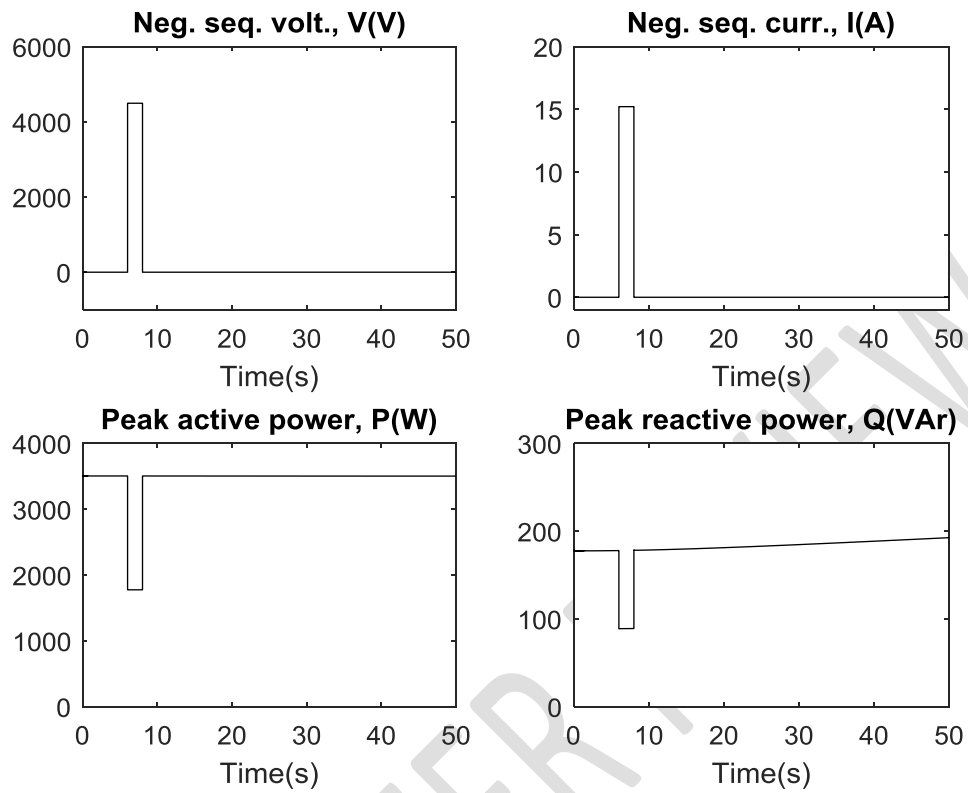


138
139
140
141
142

Fig. 9. Response of MS1 to L-L short circuit at ends of feeder-a – Q control

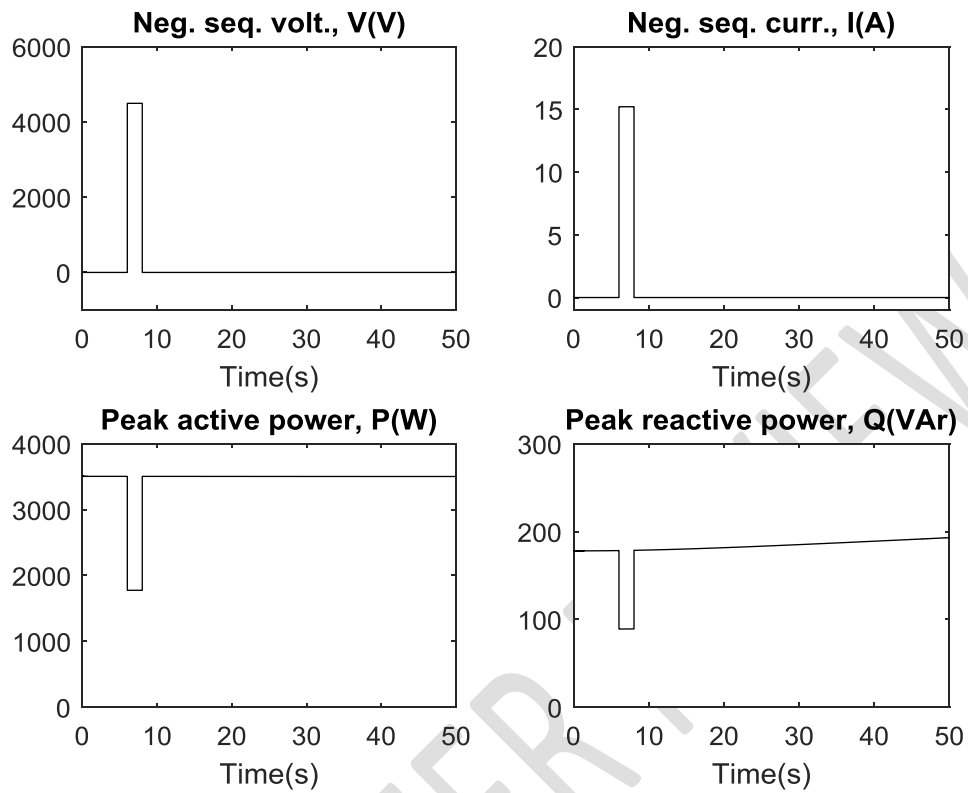
Fig. 10 shows response of feeder-a when it is short-circuited under V control, while fig. 11 shows response of same feeder to same short circuit under Q control.

$P(W)$ = Nominal active power in Watts; $Q(VAr)$ = Nominal reactive power in Volt-Amp reactive



143
 144 **Fig. 10.** Response of feeder-a when it is short-circuited – V control
 145

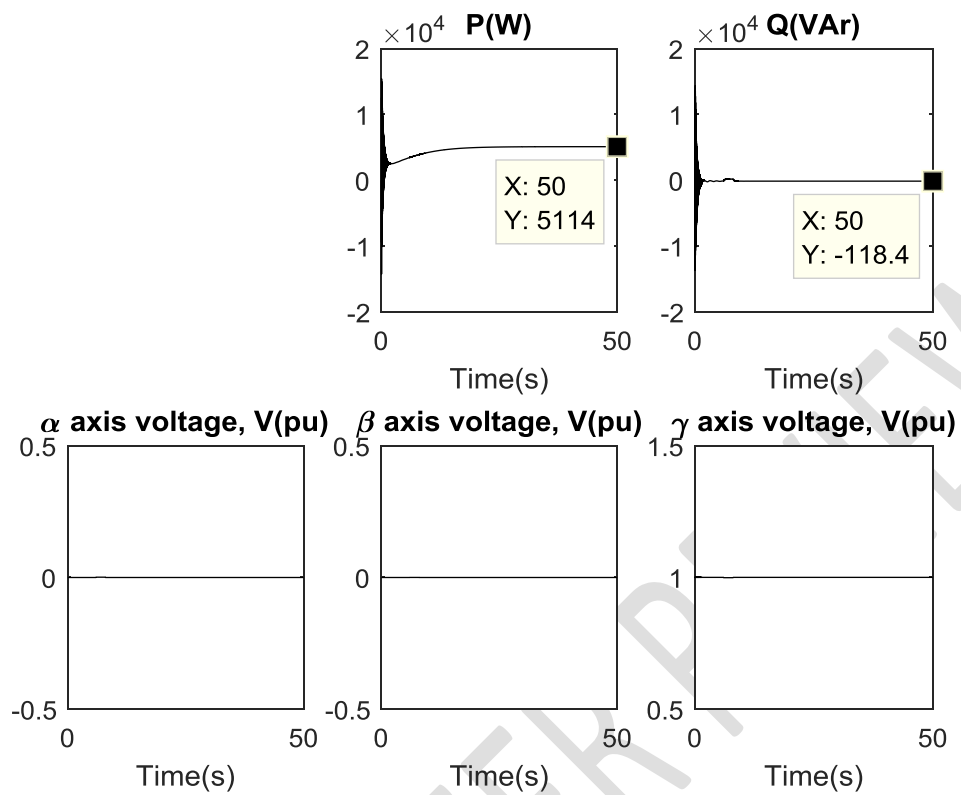
P(W) = Nominal active power in Watts; Q(VAr) = Nominal reactive power in Volt-Amp reactive



146
147 **Fig. 11.** Response of feeder-a when it is short-circuited – Q control
148

149 Fig. 12 shows response of MS2 when terminals of MS1 are short-circuited under V control,
150 while fig. 13 shows response of MS2 when terminals of MS1 are short-circuited under Q control.

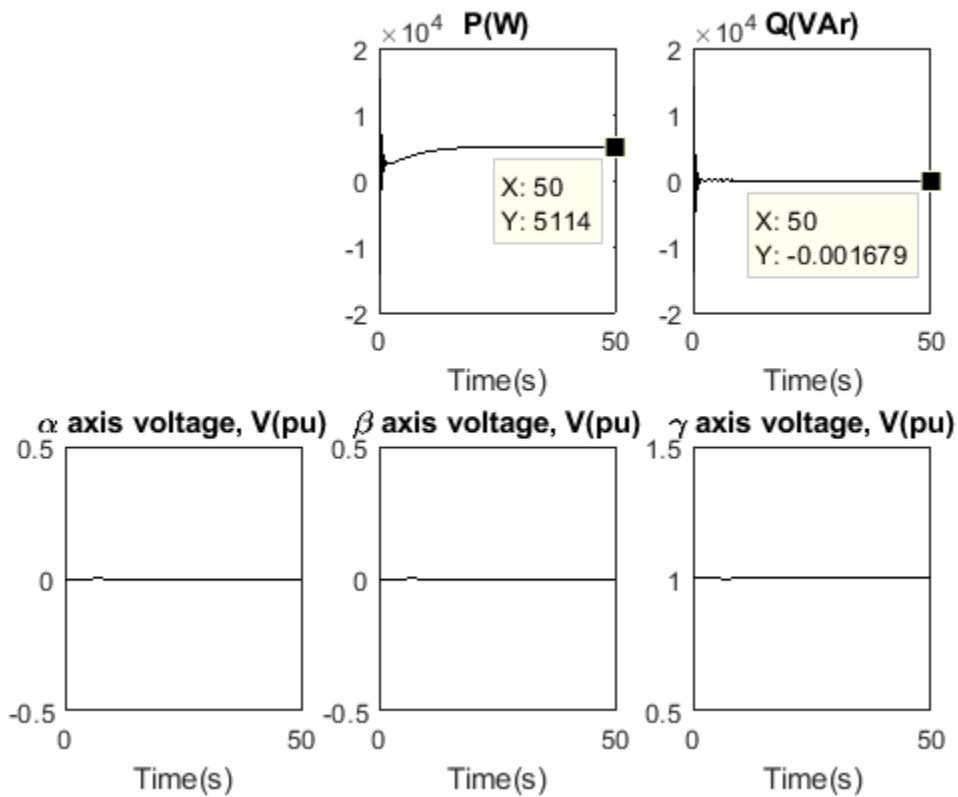
151
152



153
154
155

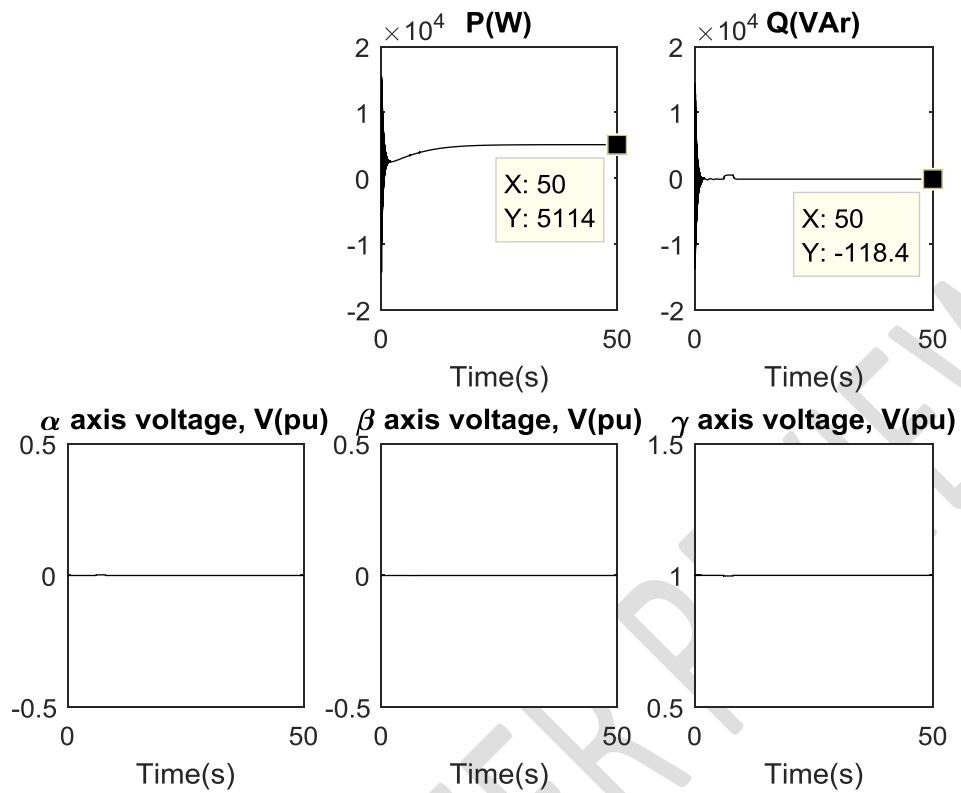
Fig. 12. Response of MS2 to L-L short circuit at terminals of MS1 – V control

$P(W)$ = Nominal active power in Watts; $Q(VAr)$ = Nominal reactive power in Volt-Amp reactive



156
157 **Fig. 13.** Response of MS2 to L-L short circuit at terminals of MS1 – Q control

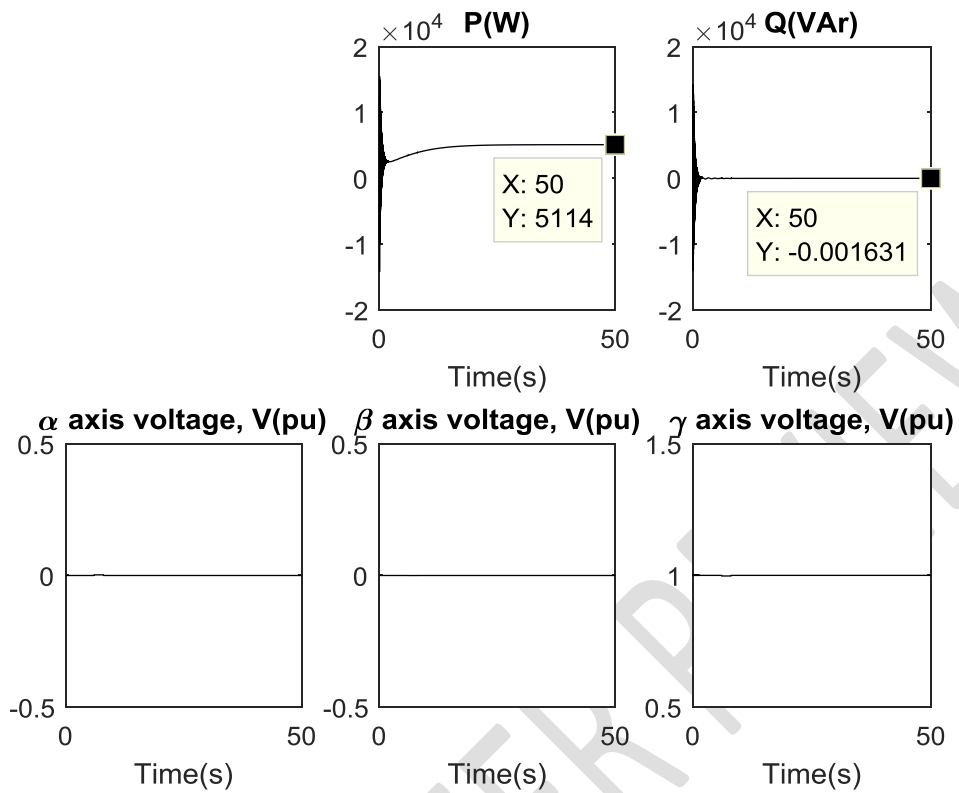
158
159 Fig. 14 shows response of MS2 when ends of feeder-a are short-circuited under V control, while
160 fig. 15 shows response of MS2 when ends of feeder-a are short-circuited under Q control.
161



162
163
164

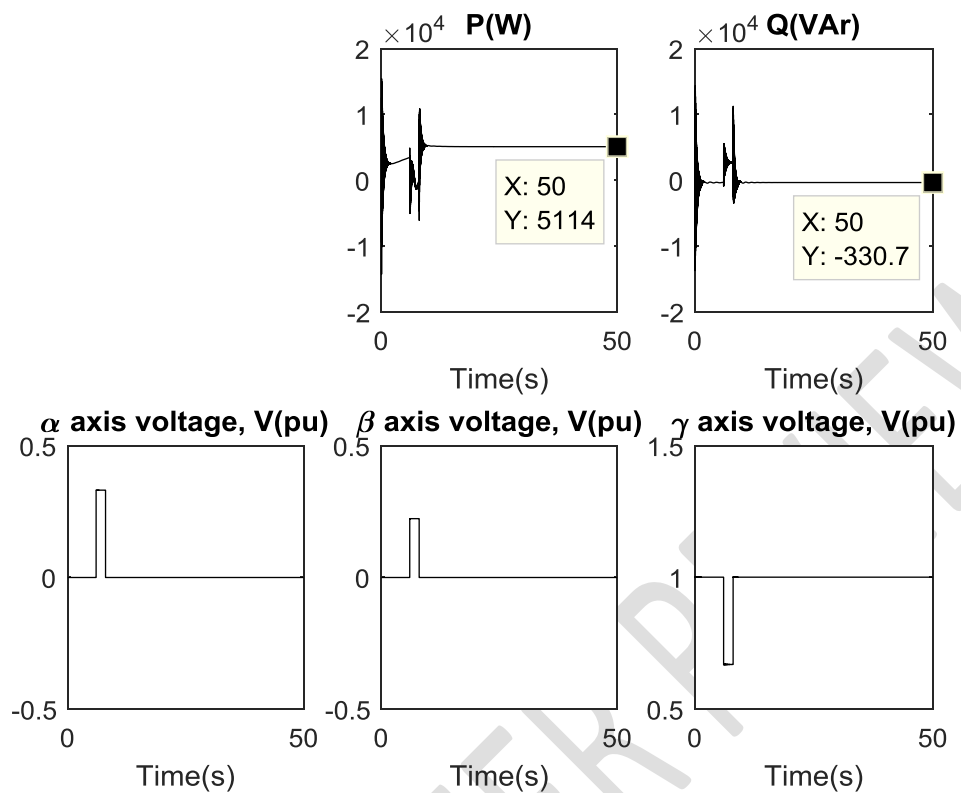
Fig. 14. Response of MS2 to L-L short circuit at ends of feeder-a – V control

$P(W)$ = Nominal active power in Watts; $Q(VAr)$ = Nominal reactive power in Volt-Amp reactive



165
166 **Fig. 15.** Response of MS2 to L-L short circuit at ends of feeder-a – Q control
167

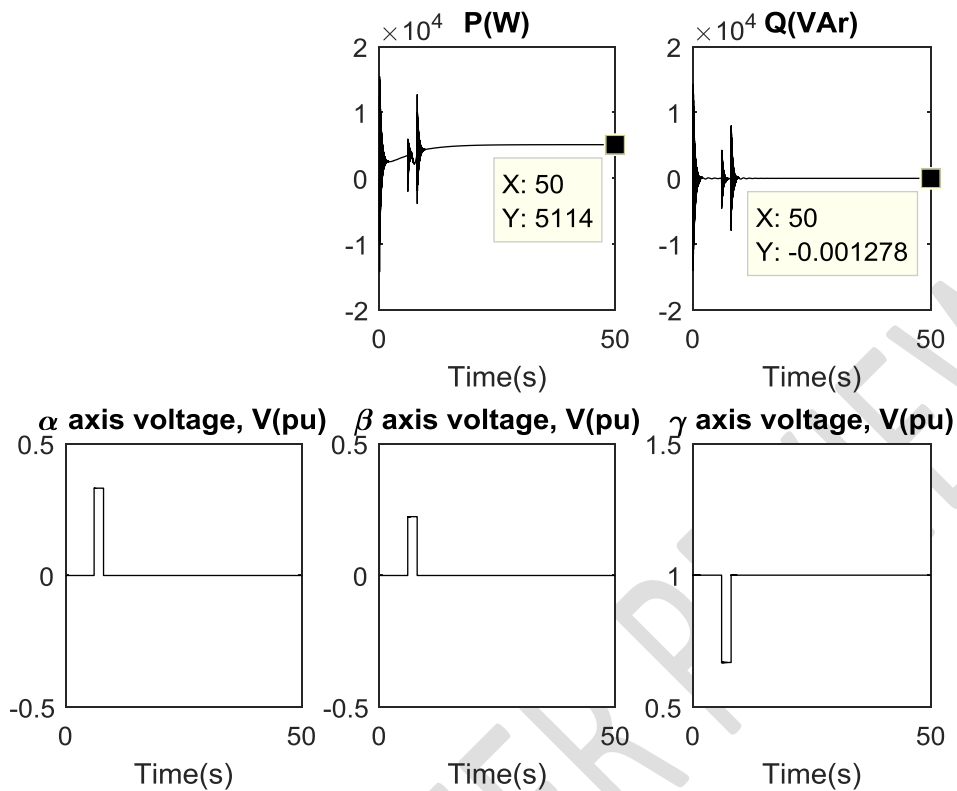
168 Fig. 16 shows response of MS1 to cross-country L-L short circuit at terminals of MS1 and MS2
169 under V control, while fig. 17 shows response of MS1 to same fault as in fig. 16 but under Q
170 control.



171
 172 **Fig. 16.** Response of MS1 to cross-country L-L short circuit at terminals of MS1 and MS2 – V
 173 control

174
 175
 176

$P(W)$ = Nominal active power in Watts; $Q(VAr)$ = Nominal reactive power in Volt-Amp reactive



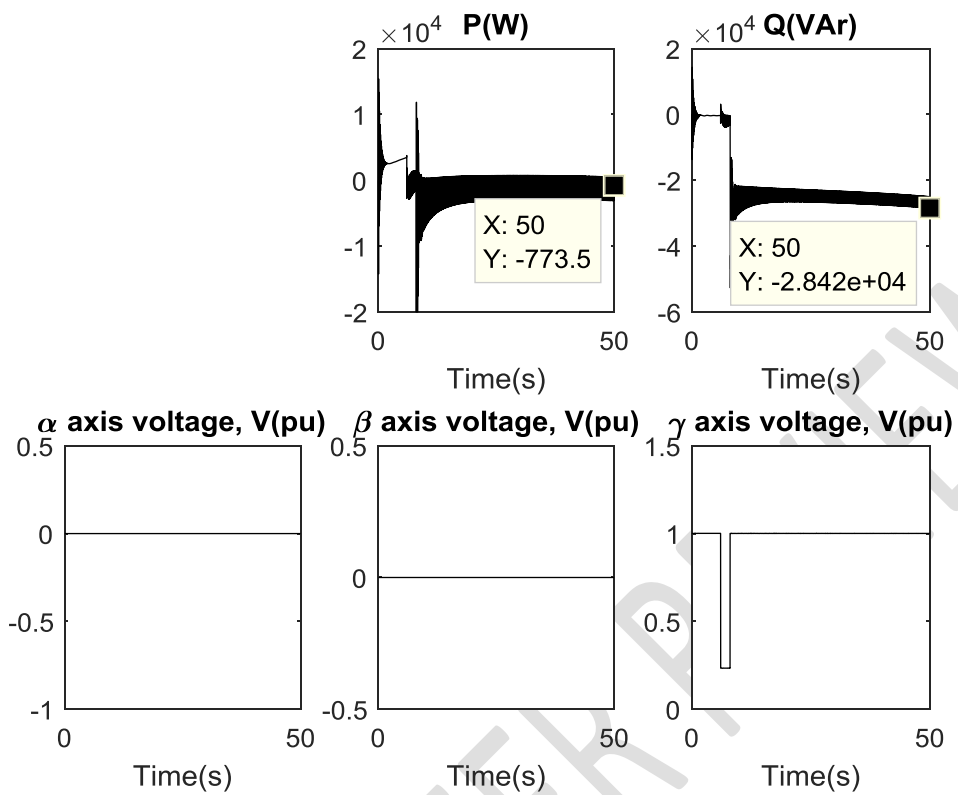
177
 178 **Fig. 17.** Response of MS1 to cross-country L-L short circuit at terminals of MS1 and MS2 – Q
 179 control

180 **6. Three phase bolted short circuit**

181 In order to present a peek into the response of the microsource as short circuit severity increases,
 182 its response to three phase bolted short circuit is presented in fig. 18 and fig. 19.

183 Fig. 18 and fig. 19 show response of MS1 when three phase-to-ground bolted short circuit is
 184 applied at its terminals under V control and Q control, respectively.

185

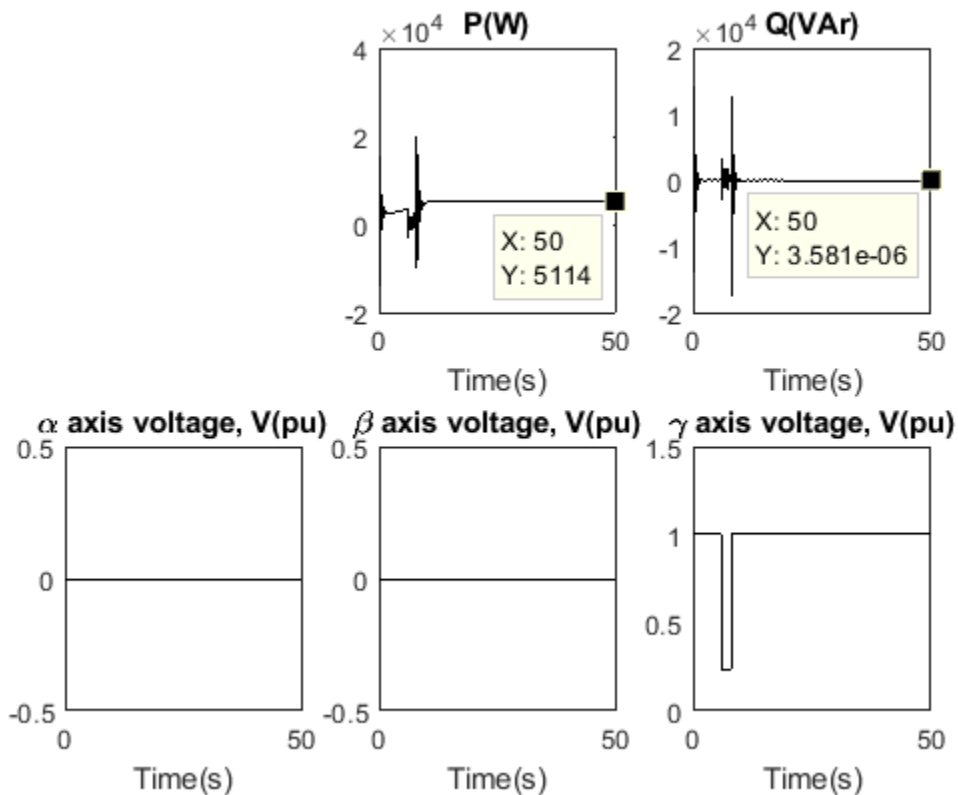


186

187 **Fig. 18.** Response of MS1 to 3-phase bolted short circuit – V control

188

$P(W)$ = Nominal active power in Watts; $Q(VAr)$ = Nominal reactive power in Volt-Amp reactive



189
190 **Fig. 19.** Response of MS1 to 3-phase bolted short circuit – Q control

191 **7. Results and discussion**

192 As observed from the simulation results, the generation of each microsource is 92% of its
193 nominal rating when operating under stress-free condition. Similarly, during normal operation,
194 absorption of reactive power of each microsource from the external reactive power compensator
195 is more under V control than Q control. This indicates DFIG's reactive support from its
196 converter dc bus under Q control. This reactive support is, however, unsustainable for continuous
197 operation since the capacitor linked to its converter dc bus is of small capacity.

198 At 50.0s, under V control (fig. 4) when L-L short circuit is applied at its terminals, MS1 absorbs
199 330.7 VAr from its reactive VAr compensator and that of MS2. This is considerably higher than
200 0.001307 VAr it absorbs under Q control (fig. 5), indicative of reactive power management of
201 DFIG as published by Moayed Moghbel et al. in [24] and in [25-27]. The peak active power of
202 feeder-a rose to 20kW in a direction opposite the nominal active power flow direction during the
203 fault, indicating active power support from MS2 and feeder-b to feed the fault point in feeder-a.
204 Similarly, reactive power flow on feeder-a rose to more than 40 kVAr in an opposite direction
205 during the fault, as seen in fig. 5. Negative sequence quantities only exist during the fault, as
206 depicted in fig. 6 and fig. 7.

207 At 50.0s, under V control (fig. 8) when L-L short circuit is applied at ends of feeder-a, MS1
208 absorbs 118.4 VAr from the reactive VAr compensators. This is considerably higher than
209 0.001627 VAr it absorbs under Q control (fig. 9), indicative of reactive power management of
210 DFIG as published by Moayed Moghbel et al. in [24] and in [28, 29]. The peak active power of

$P(W)$ = Nominal active power in Watts; $Q(VAr)$ = Nominal reactive power in Volt-Amp reactive

211 feeder-a dropped to less than 2kW during the fault. Similarly, reactive power flow on feeder-a
212 dropped to less than 100 VAR during the fault, as seen in fig. 10 and fig. 11. Negative sequence
213 quantities only exist during the fault, as depicted in fig. 9 and fig. 11.

214 At 50.0s, under V control (fig. 12) when L-L short circuit is applied at terminals of MS1, MS2
215 absorbs 118.4 VAR from the reactive VAR compensators. This is considerably higher than
216 0.001679 VAR it absorbs under Q control (fig. 13), indicating reactive power management of
217 DFIG as published by Moayed Moghbel et al. in [24] and in [28, 29]. The transformed stator
218 voltage of MS2 is undisturbed as the severity of the fault is minimized by the impedance of
219 feeder-a and feeder-b, as shown in fig. 12 to fig. 15.

220 At 50.0s, under V control (fig. 16) when cross-country L-L short circuit is applied at terminals of
221 MS1 and MS2, MS1 absorbs 330.7 VAR from the reactive VAR compensators. This is
222 considerably higher than 0.001278 VAR it absorbs under Q control (fig. 17), indicating reactive
223 power management of DFIG as published by Moayed Moghbel et al. in [24] and in [28, 29].
224 Both active and reactive power of MS1 are unstable during the fault in both V and Q control, but
225 more visible instability is observed under V control regime. Voltage and frequency instability is
226 a major challenge of microgrid operation, as published in [30-32]. During the fault, the
227 transformed stator voltages of MS1 is disrupted in the α , β and γ axes as the severity of the
228 fault is higher than L-L faults that are not cross-country, as shown in fig. 16 and fig. 17.

229 At 50.0s, under V control (fig. 18) when 3-phase bolted short circuit is applied at terminals of
230 MS1, MS1 absorbs (a change of operation from generation mode to motoring mode of DFIG)
231 0.7735kW from MS2 and also absorbs 28.42 kVAR from the reactive VAR compensators. This is
232 considerably higher than under Q control regime (fig. 19) where, with same short circuit, MS1
233 generates 5.114kW and supports the system with 3.581×10^{-6} VAR. This validates reactive power
234 management of DFIG as published by Moayed Moghbel et al. in [24] and in [28, 29]. Both active
235 and reactive power of MS1 are unstable during the fault in both V and Q control, but virulent and
236 sustained instability is observed under V control regime. Voltage and frequency instability is a
237 major challenge of microgrid operation, as published in [30-32]. The DFIG remained in
238 generation mode under Q control while it changed to motoring mode under V control when
239 exposed to 3-phase bolted short circuit. During the fault, the transformed stator voltages of MS1
240 is disrupted in the γ axis as the severity of the fault is high, as shown in fig. 18 and fig. 19.

241

242 8. Conclusion

243 The simulation results of this work has shown that when the system is under 2-second line-to-
244 line short circuit stress, bidirectional flow of active and reactive power between the two feeders
245 occurs, particularly power support at fault points. The simulation has also verified the theory of
246 power management capability of DFIG by showing that each microsource offers superior active
247 and reactive power post-fault stability under Q control than V control when the microgrid is
248 faulted. This is especially obvious as the fault severity increases due to the effect of power
249 electronic (converter and controller) interfacing of DFIG. Finally, the interaction and the
250 engagement of critical quantities in a wind turbine distributed generation with a local load has
251 been explored and depicted. Such is the α, β, γ transformation of DFIG's complex form of stator
252 voltage (a, b, c). Each set of α, β, γ plot shows a unique pattern to fault location, making the
253 α, β, γ transformation a potential candidate for fault sensing and diagnosis – regardless of

254 control regime. In conclusion, the response of the testbed to line-to-line short circuit has been
255 shown to agree with established theory. This helps validate its response to line-to-line short
256 circuit.
257

258

259 REFERENCES

- 260 [1] G. Didier, C.H. Bonnard, T. Lubin, J. Lévêque, Comparison between inductive and resistive SFCL in
261 terms of current limitation and power system transient stability, *Electric Power Systems Research*, 125
262 (2015) 150-158.
- 263 [2] D. Filipović-Grčić, B. Filipović-Grčić, K. Capuder, Modeling of three-phase autotransformer for
264 short-circuit studies, *International Journal of Electrical Power & Energy Systems*, 56 (2014) 228-234.
- 265 [3] S.V. Papaefthymiou, V.G. Lakiotis, I.D. Margaritis, S.A. Papathanassiou, Dynamic analysis of island
266 systems with wind-pumped-storage hybrid power stations, *Renewable Energy*, 74 (2015) 544-554.
- 267 [4] F. Sulla, J. Svensson, O. Samuelsson, Symmetrical and unsymmetrical short-circuit current of
268 squirrel-cage and doubly-fed induction generators, *Electric Power Systems Research*, 81 (2011) 1610-
269 1618.
- 270 [5] T.-H. Chen, W.-T. Huang, Evaluation of the variations of short-circuit capacities along a feeder due to
271 distribution system-type upgrading, *International Journal of Electrical Power & Energy Systems*, 31
272 (2009) 50-58.
- 273 [6] O.E. Roennspiess, A.E. Efthymiadis, A comparison of static and dynamic short circuit analysis
274 procedures, *IEEE Transactions on Industry Applications*, 26 (1990) 463-475.
- 275 [7] N. Soni, S. Doolla, M.C. Chandorkar, Improvement of Transient Response in Microgrids Using
276 Virtual Inertia, *IEEE Transactions on Power Delivery*, 28 (2013) 1830-1838.
- 277 [8] O. Palizban, K. Kauhaniemi, J.M. Guerrero, Microgrids in active network management – part II:
278 System operation, power quality and protection, *Renewable and Sustainable Energy Reviews*, 36 (2014)
279 440-451.
- 280 [9] I. Patrao, E. Figueres, G. Garcerá, R. González-Medina, Microgrid architectures for low voltage
281 distributed generation, *Renewable and Sustainable Energy Reviews*, 43 (2015) 415-424.
- 282 [10] O.S. Adio, L. Xiangning, Z. Feng, B. Zhiqian, Short circuit analysis for integration of 10MW
283 Windfarm in Nigeria at the PCC, in: 2013 IEEE Power and Energy Society General Meeting (PES),
284 2013, pp. 1-5.
- 285 [11] M. Chaudhary, S.M. Brahma, S.J. Ranade, Short circuit analysis of Type II induction generator and
286 wind farm, in: 2012 IEEE PES Transmission and Distribution Conference and Exposition (T&D) 2012,
287 pp. 1-5.
- 288 [12] A. Mathur, V. Pant, B. Das, Unsymmetrical short-circuit analysis for distribution system considering
289 loads, *International Journal of Electrical Power & Energy Systems*, 70 (2015) 27-38.
- 290 [13] N. Samaan, R. Zavadil, J.C. Smith, J. Conto, Modeling of wind power plants for short circuit
291 analysis in the transmission network, in: Transmission and Distribution Conference and Exposition,
292 2008. T&D;D. IEEE/PES, 2008, pp. 1-7.
- 293 [14] N. Hatzargyriou, H. Asano, R. Iravani, C. Marnay, Microgrids, *IEEE Power and Energy Magazine*,
294 5 (2007) 78-94.
- 295 [15] J.W.B. Jan Machowski, James R. Bumby, *Power System Dynamics and Stability*, John Wiley &
296 Sons, England, 1997.
- 297 [16] R.H. Lasseter, MicroGrids, in: 2002 IEEE Power Engineering Society Winter Meeting, 2002, pp.
298 305-308 vol.301.
- 299 [17] R.J. Best, D.J. Morrow, P.A. Crossley, Current transients in the small salient-pole alternator during
300 sudden short-circuit and synchronisation events, *IET Electric Power Applications*, 4 (2010) 687-700.

P(W) = Nominal active power in Watts; Q(VAr) = Nominal reactive power in Volt-Amp reactive

- 301 [18] W.H. Kersting, G. Shirek, Short circuit analysis of IEEE test feeders, in: 2012 IEEE PES
302 Transmission and Distribution Conference and Exposition (T&D) 2012, pp. 1-9.
- 303 [19] J. Ouyang, X. Xiong, Research on short-circuit current of doubly fed induction generator under non-
304 deep voltage drop, *Electric Power Systems Research*, 107 (2014) 158-166.
- 305 [20] J. Prajapati, V. Patel, H. Patel, Load flow, short circuit and stability analysis using Matlab, in: *Green*
306 *Computing Communication and Electrical Engineering (ICGCCEE)*, 2014 International Conference on,
307 2014, pp. 1-5.
- 308 [21] A. Bracale, P. Caramia, A.R. Di Fazio, D. Proto, Probabilistic short circuit analysis in electric power
309 distribution systems including distributed generation, in: *8th Mediterranean Conference on Power*
310 *Generation, Transmission, Distribution and Energy Conversion (MEDPOWER 2012)*, 2012, pp. 1-6.
- 311 [22] T. Jen-Hao, Unsymmetrical Short-Circuit Fault Analysis for Weakly Meshed Distribution Systems,
312 *IEEE Transactions on Power Systems*, 25 (2010) 96-105.
- 313 [23] J. Ouyang, X. Xiong, Dynamic behavior of the excitation circuit of a doubly-fed induction generator
314 under a symmetrical voltage drop, *Renewable Energy*, 71 (2014) 629-638.
- 315 [24] M. Moghbel, H.T. Mokui, M.A.S. Masoum, M. Mohseni, Reactive power control of DFIG wind
316 power system connected to IEEE 14 bus distribution network, in: *Universities Power Engineering*
317 *Conference (AUPEC)*, 2012 22nd Australasian, 2012, pp. 1-7.
- 318 [25] X. Dongliang, X. Zhao, Y. Lihui, J. Ostergaard, X. Yusheng, W. Kit Po, A Comprehensive LVRT
319 Control Strategy for DFIG Wind Turbines With Enhanced Reactive Power Support, *IEEE Transactions*
320 *on Power Systems*, 28 (2013) 3302-3310.
- 321 [26] J. Jeong-Ik, K. Young-Sin, L. Dong-Choon, Active and Reactive Power Control of DFIG for Wind
322 Energy Conversion under Unbalanced Grid Voltage, in: *IEEE 5th International Power Electronics and*
323 *Motion Control Conference 2006, IPERC 2006*, 2006, pp. 1-5.
- 324 [27] M. Kayikci, J.V. Milanovic, Reactive Power Control Strategies for DFIG-Based Plants, *IEEE*
325 *Transactions on Energy Conversion*, 22 (2007) 389-396.
- 326 [28] S.A. Gopalan, V. Sreeram, H.H.C. Iu, A review of coordination strategies and protection schemes for
327 microgrids, *Renewable and Sustainable Energy Reviews*, 32 (2014) 222-228.
- 328 [29] E. Planas, A. Gil-de-Muro, J. Andreu, I. Kortabarria, I. Martínez de Alegría, General aspects,
329 hierarchical controls and droop methods in microgrids: A review, *Renewable and Sustainable Energy*
330 *Reviews*, 17 (2013) 147-159.
- 331 [30] R. Romo, O. Micheloud, Power quality of actual grids with plug-in electric vehicles in presence of
332 renewables and micro-grids, *Renewable and Sustainable Energy Reviews*, 46 (2015) 189-200.
- 333 [31] M. Soshinskaya, W.H.J. Crijns-Graus, J.M. Guerrero, J.C. Vasquez, Microgrids: Experiences,
334 barriers and success factors, *Renewable and Sustainable Energy Reviews*, 40 (2014) 659-672.
- 335 [32] R. Zamora, A.K. Srivastava, Controls for microgrids with storage: Review, challenges, and research
336 needs, *Renewable and Sustainable Energy Reviews*, 14 (2010) 2009-2018.

337